Optics Letters

Photoacoustic resonance by spatial filtering of focused ultrasound transducers

Dongyel Kang,[1,*] Bahman Lashkari,[2] and Andreas Mandelis[2]

[1]School of Basic Sciences, College of Engineering, Hanbat National University, Daejeon, South Korea
[2]Center for Advanced Diffusion-Wave and Photoacoustic Technologies (CADIPT), Department of Mechanical and Industrial Engineering, University of Toronto, 5 King's College Road, Toronto, Ontario M5S 3G8, Canada
*Corresponding author: dkang@optics.arizona.edu

Received 1 December 2016; revised 18 December 2016; accepted 27 December 2016; posted 11 January 2017 (Doc. ID 281791); published 2 February 2017

The effect of a spherically focused ultrasound (US) transducer (TD) on photoacoustic (PA) measurements is analytically investigated using the concept of a virtual point detector. The derived analytical results indicate that the limited numerical aperture (NA) of the PA detector takes on the role of spatial filtering of the induced PA waves, which leads to the occurrence of a peak frequency in the PA spectrum. The mathematical description of this phenomenon is similar to the result of resonance peaks of light propagation in dielectrics. This PA resonance peak depends on the NA of the US TD and the absorption coefficient of the PA source. Experimentally measured PA spectra from an ink solution using a frequency-domain PA system verify the PA resonance effect. Finally, we discuss the possibility that previously reported PA resonances interpreted as PA source viscosity might be actually caused by the US TD's spatial filtering.

OCIS codes: (260.5740) Resonance; (170.5120) Photoacoustic imaging.

https://doi.org/10.1364/OL.42.000655

The photoacoustic (PA) effect is the generation of acoustic (or ultrasound) waves from the temporal variation of thermoelastic expansion caused by photon-absorbed heating [1–3]. Because of acoustic wave characteristics, such as several orders of magnitude less scattering in biological tissue than visible-wavelength optical waves, it is possible to generate high contrast and resolution PA images of absorbing objects buried in diffusive media [1–4]. Also, spectroscopic absorption measurements by illuminating multiple-wavelength optical sources produce PA functional imaging [4,5]. These benefits of PA imaging compared to visible-wavelength optical diffusive imaging have spurred PA research in various biological applications [2–6].

Like other imaging modalities, a PA system converts PA waves induced in an object space into PA data in an image space. Since this mapping cannot be ideal, it is important to investigate the relationship between an object signal and measured data. Typically, an ultrasound (US) transducer (TD) measures PA waves induced by either nanosecond-pulsed or intensity-modulated laser beams [3–7]. In addition to the US TD's temporal response (i.e., transfer function) due to the limited spectral bandwidth, the geometrical shape of the transducer surface (spherical, planar, or cylindrical) definitely affects the characteristics of the measured PA data and thus the overall performance of PA imaging [8]. Although a cylindrically focused US TD can be considered due to its line focusing functionality [9], a spherically focused US TD has been commonly used in most PA applications [2,4]. For example, since the numerical aperture (NA) of a focused US TD is proportional to a lateral resolution of the acquired PA images, a high-NA, focused US TD is inherently used in photoacoustic microscopy to achieve a few tens of micrometers of lateral resolution [2]. Also, in typical biological applications, it is required to target some specific objects, such as a single blood vessel, bone, cancer, and other absorbers buried in highly scattering media [6,10,11] because incident photons are strongly diffused so that wide-spatial-range PA waves are induced by absorbers in the path of those diffused photons. For all those situations, it is advantageous to use an US TD with a spherically focused shape to target a local area of an object and/or effectively collect PA waves. Even for indirect PA imaging, such as PA tomography, it has been reported that PA data acquisition by spherically focused US TDs deliver better performance than other geometrical shapes of US TDs [12].

In this Letter, the effect of a spherically focused US TD on measured PA data is analytically investigated with the combined concept of a virtual point detector (VPD) and a Green's function approach. The VPD concept adapted from synthetic aperture focusing was introduced to improve the degraded lateral resolution of PA images [13], which basically assumes that a PA measurement mechanism by a spherically focused US TD is physically similar to that by the VPD located on the focal point of the US TD. Considering the coherence weighting factor and time of flight of PA waves to the VPD, the degraded lateral resolution in PA microscopy was experimentally improved [14]. In a conventional Green's function approach, PA values at each measurement point are calculated by superposing PA fields from the entire PA source area [1,15], and those superposed PA values are integrated for the entire

physical shape of a US TD. Thus, the Green function solution is expressed as a 6-dimensional integration that usually cannot lead to an analytical expression to aid physical insight. Because of this, the earlier literature considering Green's functions usually dealt with numerical calculations or assumptions of unrealistically limited PA sources, such as a point source [3,16,17].

In this Letter, consideration of the VPD within a Green function approach derives an analytical solution of PA data measured by a spherically focused US TD for a widely extended PA source. The result indicates that a peak frequency component exists in the PA spectrum due to the finite NA of US TDs, which has not been reported in the previous literature.

Figure 1 shows the conceptual schematic for PA measurements using a spherically focused US TD. The gray and pink regions indicate homogeneous background and absorbing media; μ_{eff} and μ_a are the effective scattering and absorption coefficients, respectively. The focused US TD is conceptually drawn to be located inside the background scattering medium under the assumption that the optical property of a US-matching material between the medium and US TD is the same as that of the medium. Considering spherical coordinates, as indicated by the polar angle, θ, and the two crossed dotted lines in Fig. 1, the Green function solution from the Helmholtz PA wave equation for the observation point, $\vec{r}_d$, can be written as [8,16]

$$\tilde{p}(\vec{r}_d,\omega) = \frac{i\omega\Gamma}{4\pi v_s^2}\int_V \frac{\exp[-ik|\vec{r}_d-\vec{r}|]}{|\vec{r}_d-\vec{r}|}\tilde{H}(\vec{r},\omega)\mathrm{d}V, \quad (1)$$

where Γ and v_s are the Grüneisen coefficient and ultrasound speed, respectively, both assumed to be constant. The coordinate vector, $\vec{r}$ in the integration covers the entire PA source that is characterized with the heat distribution spectrum, $\tilde{H}(\vec{r},\omega)$. For simplicity but without loss of generality, it is assumed that incident photons are uniformly distributed at the boundary between two media due to the background scattering. Thus, regarding Beer's law, the heat distribution spectrum in the semi-infinite absorption medium can be described as

$$\tilde{H}(\vec{r},\omega) = \mu_a\tilde{I}(\omega)e^{-\mu_{\text{eff}}L}\exp[-\mu_a r\cos(\pi-\theta)], \quad (2)$$

where $\tilde{I}(\omega)$ is the Fourier spectrum of the incident optical beam. Later on, we will consider two more irradiance distributions to complement the assumption of the fixed irradiance of Eq. (2).

In order to derive an analytical expression for the PA spectrum measured by the focused US TD, the concept of a VPD is introduced as indicated with the red dot in Fig. 1. Physically, only PA waves passing through the VPD can constructively contribute to a PA signal measured by the US TD. In other words, PA waves reaching the US TD without passing through the VPD destructively interfere due to phase mismatching. With this configuration, the Green function solution of Eq. (1) can be further developed with $\vec{r}_d = 0$ for the VPD and the integration range is limited to the cone shape in the PA object of Fig. 1, which is

$$\tilde{p}_{VD}(\omega) = \frac{i\omega\Gamma}{4\pi v_s^2}\int_0^{2\pi}\int_{\pi-\theta_{\text{NA}}}^{\pi}\int_0^{\infty}\frac{\exp[-ikr]}{r} \times \tilde{H}(r,\omega)r^2\sin\theta\mathrm{d}r\mathrm{d}\theta\mathrm{d}\varphi. \quad (3)$$

The integrations for variables r, θ, and ϕ in Eq. (3) are analytically performed with the substitution of Eq. (2) for $\tilde{H}(\omega)$. The result with the additional phase term, e^{-ikL}, due to PA wave propagation from the VPD to the focused US TD surface is

$$\tilde{p}(\omega) = \frac{\Gamma}{2}e^{-\mu_{\text{eff}}L}e^{-ikL}\tilde{I}(\omega)\frac{\omega}{v_s}\left[\frac{1}{i\mu_a v_s-\omega}-\frac{1}{i\mu_a v_s\cos\theta_{\text{NA}}-\omega}\right], \quad (4)$$

where $k = \omega/v_s$. Note that Eq. (4) contains the NA information of the focused US TD. For $\theta_{\text{NA}} = 0$ in Eq. (4), $\tilde{p}(\omega) = 0$. If $\theta_{\text{NA}} = \pi/2$ (i.e., NA = 1) is assumed, the result becomes the same as the previously published result [18]. Equation (4) can be rewritten as follows in order to investigate its physical meaning:

$$\tilde{p}(\omega) = \frac{\Gamma}{2}\tilde{I}(\omega)e^{-\mu_{\text{eff}}L}e^{-ikL}\frac{\omega}{v_s}\left[\frac{i\mu_a v_s(\cos\theta_{\text{NA}}-1)}{\omega^2-\omega_0^2-i\gamma\omega}\right], \quad (5)$$

where

$$\omega_0 = \mu_a v_s\sqrt{\cos\theta_{\text{NA}}} \quad \text{and} \quad \gamma = \mu_a v_s(1+\cos\theta_{\text{NA}}). \quad (6)$$

The structure of Eqs. (5) and (6) is very similar to the well-known equation describing light propagation in isotropic dielectrics [19]. In the interaction between light and dielectrics, resonance frequencies are observed due to light absorption corresponding to bound electron excitation in dielectrics. Likewise, Eq. (5) implies the existence of a resonance angular frequency ω_0 of Eq. (6) in the PA spectrum due to the PA signal generation mechanism by photon-absorbed heating. Also, the term γ in Eq. (6) is related to the bandwidth of the PA spectrum, which is similar to light interaction in dielectrics. Normalized PA spectra simulated from Eq. (4) are shown in Fig. 2 with different NA and μ_a values, where the speed of the acoustic wave, v_s, is set to 1500 m/s. The unrealistic case of NA = 1 is also shown in Fig. 2 because the result of this condition has been commonly used in the previous literature. As observed in Fig. 2, PA resonance peaks clearly exist for NAs < 1 at angular frequencies that exactly agree with ω_0 in Eq. (6). Since the generation of PA waves is based on a photon-absorbing mechanism similar to light absorption in dielectrics, the occurrence of resonance peaks in PA spectra is intuitively expected. The resonance frequency

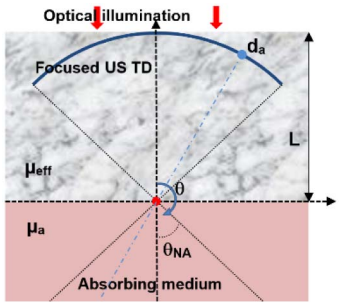

Fig. 1. Conceptual schematic of measuring PA signals using a spherically focused US TD.

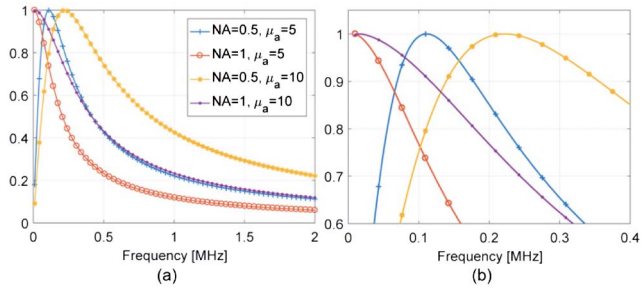

Fig. 2. (a) Simulated normalized PA spectra with different NA and μ_a values. (b) Enlarged part of (a). Units for μ_a are cm^{-1}.

dependence on the NA of the US TDs can be explained with the aid of Fig. 1. In that figure, the local PA source along the blue dashed–dotted line contributes to a PA signal through the specific point, d_a, of the US TD. The effective spatial length of each local PA source compared to the central wavelength of the generated PA waves is directly related to the spectral contribution to measured PA signals. For local PA sources near the vertical coordinate line in Fig. 1, the spatial lengths are effectively reduced because of the exponentially attenuated irradiance of Eq. (2). For local PA sources far from the vertical coordinate line, however, PA waves destructively interfere by themselves due to relatively long spatial lengths, which contribute low-frequency components, including a DC term to the PA signal. Therefore, spatial filtering by a limited NA of US TDs physically operates as a frequency filter to the measured PA spectrum, which reveals the PA resonance peak by the decrease in the low-frequency components.

It is purposeful to investigate the PA resonance phenomenon with heat distributions other than the exponentially attenuated profile of Eq. (2). To derive analytical expressions for physical insight, we consider specific mathematical descriptions for the heat distribution in the semi-infinite absorbing medium, which are

$$\tilde{H}(\vec{r},\omega) = \mu_a \tilde{I}(\omega) e^{-\mu_{\text{eff}} l} \exp[-\mu_a r] \tag{7}$$

and

$$\tilde{H}(\vec{r},\omega) = \mu_a \tilde{I}(\omega) e^{-\mu_{\text{eff}} l} \exp\{-\mu_a r[2\cos(\pi-\theta)-1]\}. \tag{8}$$

The normalized cross-sectional images of irradiance distributions of Eqs. (7) and (8) are shown for clarity in Figs. 3(a) and 3(b), respectively. The dark regions at the top of each figure indicate the homogeneous background medium in Fig. 1. A focused optical illumination for concentrating more photon energy on a central absorbing area can generate irradiance distributions like Fig. 3(a). Irradiances similar to Fig. 3(b) can be realized by a ring-type optical illumination that has been used in PA microscopy to avoid strong PA signals around the central surface of absorbing media [2]. Substituting Eqs. (7) and (8) into Eq. (3) leads to the same mathematical description as Eq. (5) with differently defined quantities of ω_0 and γ, as follows:

$$\omega_0 = \mu_a v_s \quad \text{and} \quad \gamma = 2\mu_a v_s \tag{9}$$

for Eq. (7) and

$$\omega_0 = \mu_a v_s \sqrt{2\cos\theta_{\text{NA}} - 1} \quad \text{and} \quad \gamma = \mu_a v_s (2\cos\theta_{\text{NA}}) \tag{10}$$

for Eq. (8). Equations (9) and (10) indicate the general existence of PA resonance frequencies in PA spectra measured with a focused US TDs regardless of heat distributions. Also, they show that the PA resonance frequency values are increased for Eq. (7) and decreased for Eq. (8) compared with Eq. (2) for a fixed NA.

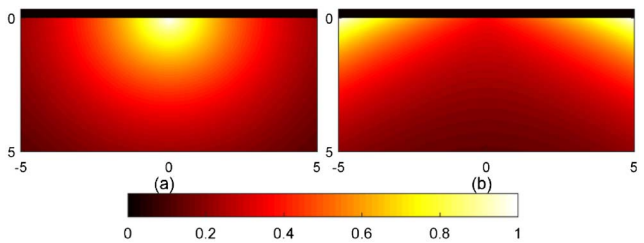

Fig. 3. Normalized irradiance distributions of Eqs. (7) and (8), respectively.

This can be easily explained from the concept of spectral contribution of local PA sources explained in the previous paragraph. For example, the frequency components of local PA sources in high-NA areas tend to be increased for the heat distribution of Eq. (7) compared with the case of Eq. (3) because of the reduced spatial length from the more rapid irradiance attenuation.

Experiments verifying the PA resonance were conducted with a frequency-domain (FD) PA system [6,20]. The wavelength and power of the laser illumination (LDX-3230-680, RPMC) in the system were 680 nm and ~650 mW, respectively. The focal length and NA of the focused US TD (V305-SU, Olympus, 2.25 MHz) used in the experiment were 1 in. and 0.375. The homemade LabVIEW program controlling the analog–digital convertor board (NI-PXIe-5122) and function generator (33522B, Agilent) processed cross-correlations between the reference signals and the measured PA data induced by chirped optical illumination. The detailed description and concept of the FD PA system can be found elsewhere [18,20]. Although the PA resonance theory was derived for the reflection-mode PA measurement as described in Fig. 1, the experiment was conducted in the transmission mode (i.e., the US TD in Fig. 1 is located on the bottom) in order to increase an absorbed optical power and alignment reliability. For PA measurements with a spherically focused US TDs, it is theoretically verified that PA signals for these two modes are mirror images of each other in the time domain, which means PA spectra are the same except for some constant phase terms [21]. The absorbing medium was realized with an ink–water solution in the ~100 mm × 100 mm × 13 mm container where there are open windows on each wall sealed by a thin plastic wrap. The absorption coefficients of ink solutions were measured in another experiment where Beer's law was applied to measurements of laser transmittance through a quartz spectrophotometer cell (45-Q-2, Starna Cells, Inc.) before and after filling it with the ink solutions.

Normalized PA spectra by Fourier transforming real FD PA signals from two independently performed experiments are shown in Fig. 4. Both results with insets showing magnified parts clearly verify the existence of PA resonance peaks. There are two main differences from theoretical expectations in the experimental results. First, experimentally acquired PA resonance values are higher than ω_0 in Eq. (6). In the PA spectrum calculation for Fig. 4, PA signals in the time window of 12–20 μs were considered in order to remove contaminated parts by radio-frequency noise and randomly reflected PA waves in the short and long time ranges, respectively. To investigate the effect of the limited time window on calculating PA spectra, brute-force simulations were performed, as shown in

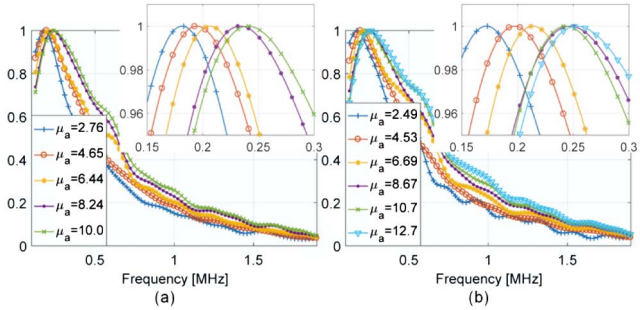

Fig. 4. Experimentally measured normalized PA spectra with insets for magnified regions around PA resonance peaks. Units for μ_a are cm^{-1}.

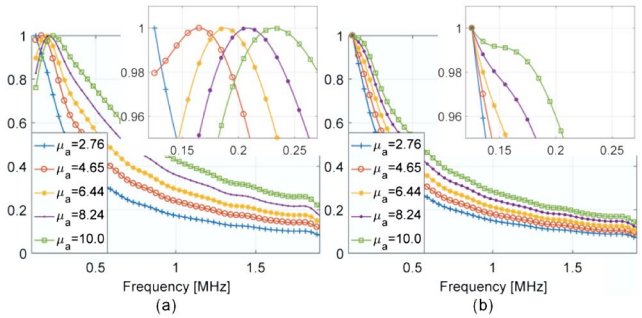

Fig. 5. Normalized PA spectra calculated from simulated PA signals for (a) NA = 0.375 and (b) NA = 1. Units for μ_a are cm^{-1}.

Fig. 5. Here, PA signals were directly simulated from Eq. (5). Then, the exact same Fourier transform processes as done for Fig. 4 were applied to those simulated signals with the limited time window. Figure 5(a) shows that the simulated PA spectra exhibit the tendency of higher peak frequency values than ω_0 in Eq. (6) similar to Fig. 4(a). Although not shown here, it is observed that those simulated PA resonance values approach the ω_0 in Eq. (6) as the time window length is increased. Also, Fig. 5(b) clearly shows that the PA resonance peaks disappear for NA = 1, which validates the spatial filtering of focused US TDs as the source of the PA resonance. Second, for the range of high absorption coefficients in Fig. 4, resonance peaks seem to be saturated rather than proportionally increased as expected in Eq. (6). Because of wave diffraction in experimental situations, which is omitted in the VPD concept, the PA source area near the VPD becomes a cylindrical shape, not a cone shape, as known as a US TD focal zone [2,12]. As the absorption coefficient is increased, the PA signal is increasingly contributed from the focal zone area due to the reduced optical penetration depth. As a result, the spatial filtering effect of a focused US TD is diminished inside the cylindrical-shaped focal zone, which leads to the saturation of PA resonance frequencies.

Previously, the PA resonance phenomenon showing peaks in PA spectra was experimentally observed by some research groups [22–24]. They theoretically interpreted the experimentally observed PA resonance with the PA source viscosity, which is mainly related to the damping term in the PA wave equation. However, it is well known that the effect of viscosity on PA measurements is almost negligible in most liquid-type PA sources [15]. To circumvent this discrepancy, the authors introduced a propagation phase constant, ρ, under the assumption that the PA pressure is in the specific form of $e^{i\rho x}P(t)$ [22]. However, it is controversial that the spatial part of a PA pressure could be described by the single phase constant against a wide PA spectrum. Furthermore, starting from this assumption, they concluded that the PA source viscosity critically affects PA resonance frequency values. As experimentally verified in Fig. 4, however, peak frequencies are significantly different for different concentrations of ink solutions. Those concentrations are obtained by adding just a few milliliters of ink into a few hundred milliliters of water, which indicates that the viscosity values of all ink solutions are almost the same. Therefore, it appears likely that previously observed PA resonance phenomena were also caused by spatial filtering of US TDs.

In this Letter, we developed the theory for PA signals measured with a focused UD TD using the combined concept of a VPD and Green function formalism. The theory implies that the frequency filtering by a finite NA of the US TD causes the occurrence of the PA resonance phenomenon, which is experimentally verified in the FD PA system. Since all US TDs used in real PA measurements inherently have a spatially limited field of view (e.g., even a point-type US TD, such as a hydrophone, has a limited measurement solid angle), we believe it is worth investigating further the spatial filtering effect on PA measurements to effectively characterize and optimize PA systems for imaging applications.

Funding. National Research Foundation of Korea (NRF), Ministry of Education (MOE) (2014R1A1A2057982); Natural Sciences and Engineering Research Council of Canada (NSERC); Canadian Institutes of Health Research (CIHR); Collaborative Health Research Project (CHRP) (CPG-127781).

Acknowledgment. A. Mandelis and B. Lashkari acknowledge the CHRP grant to A.M. and Stuart Foster (Sunnybrook Hospital).

REFERENCES

1. G. J. Diebold, T. Sun, and M. I. Khan, Phys. Rev. Lett. **67**, 3384 (1991).
2. H. F. Zhang, K. Maslov, G. Stoica, and L. V. Wang, Nat. Biotechnol. **24**, 848 (2006).
3. C. Li and L. V. Wang, Phys. Med. Biol. **54**, R59 (2009).
4. S. Mallidi, G. P. Luke, and S. Emelianov, Trends Biotechnol. **29**, 213 (2011).
5. D. Kang, Q. Huang, and Y. Li, Biomed. Opt. Express **6**, 536 (2015).
6. B. Lashkari and A. Mandelis, J. Biomed. Opt. **19**, 036015 (2014).
7. B. Lashkari and A. Mandelis, Opt. Lett. **35**, 1623 (2010).
8. M. Xu and L. V. Wang, Phys. Rev. E **67**, 056605 (2003).
9. D. Queirós, X. L. Déan-Ben, A. Buehler, D. Razansky, A. Rosenthal, and V. Ntziachristos, J. Biomed. Opt. **18**, 076014 (2013).
10. D. Kang, Q. Huang, and Y. Li, Biomed. Opt. Express **5**, 1445 (2014).
11. L. Yang, B. Lashkari, J. W. Y. Tan, and A. Mandelis, J. Biomed. Opt. **20**, 076016 (2015).
12. C. Li and L. V. Wang, Appl. Phys. Lett. **93**, 033902 (2008).
13. C.-K. Liao, M.-L. Li, and P.-C. Li, Opt. Lett. **29**, 2506 (2004).
14. M. Li, H. F. Zhang, K. Maslov, G. Stoica, and L. V. Wang, Opt. Lett. **31**, 474 (2006).
15. H. H. Barrett and K. J. Myers, *Foundations of Image Science* (Wiley, 2004).
16. A. R. Fisher, A. J. Schissler, and J. C. Schotland, Phys. Rev. E **76**, 1 (2007).
17. A. Petschke and P. J. La Rivière, Biomed. Opt. Express **1**, 1188 (2010).
18. B. Lashkari and A. Mandelis, J. Acoust. Soc. Am. **130**, 1313 (2011).
19. G. R. Fowles, *Introduction to Modern Optics*, 2nd ed. (Holt, Rinehart and Winston, 1957).
20. S. Telenkov, A. Mandelis, B. Lashkari, and M. Forcht, J. Appl. Phys. **105**, 102029 (2009).
21. H. Seok and D. Kang are preparing a manuscript to be titled "Analysis for photoacoustic measurements of transmittance and reflection modes."
22. C. Lou and D. Xing, Appl. Phys. Lett. **96**, 211102 (2010).
23. F. Gao, Y. Zheng, X. Feng, and C.-D. Ohl, Appl. Phys. Lett. **102**, 1 (2013).
24. F. Gao, Y. Zheng, X. Feng, and C.-D. Ohl, J. Biomed. Opt. **19**, 067006 (2014).